Improved Simulation of Florida Summer Convection Using the PLACE Land Model and a 1.5-Order Turbulence Parameterization Coupled to the Penn State–NCAR Mesoscale Model

BARRY H. LYNN,* DAVID R. STAUFFER,+ PETER J. WETZEL,# WEI-KUO TAO,# PINHAS ALPERT,@ NATALY PERLIN,@ R. DAVID BAKER,& RICARDO MUÑOZ,+ AARON BOONE,** AND YIQIN JIA++

*Columbia University Center for Climate System Research, New York, New York, and Mesoscale Atmospheric Processes Branch, NASA Goddard Space Flight Center, Greenbelt, Maryland
+Department of Meteorology, The Pennsylvania State University, University Park, Pennsylvania
#Mesoscale Atmospheric Processes Branch, NASA Goddard Space Flight Center, Greenbelt, Maryland
@Department of Geophysics and Planetary Sciences, Tel Aviv University, Tel Aviv, Israel
&Universities Space Research Association, Mesoscale Atmospheric Processes Branch, Greenbelt, Maryland
**CNRM/Météo France, Toulouse, France
++Science Systems and Applications Inc., Mesoscale Atmospheric Processes Branch, Greenbelt, Maryland

(Manuscript received 21 September 1999, in final form 17 August 2000)

ABSTRACT

Three major modifications to the treatment of land surface processes in the Pennsylvania State University–National Center for Atmospheric Research mesoscale model MM5, are tested in a matrix of eight model experiments. Paired together in each dimension of the matrix are versions of the code with and without one of the changes. The three changes involve 1) a sophisticated land surface model [the Parameterization for Land–Atmosphere Convective Exchange (PLACE)], 2) the soil moisture and temperature initial conditions derived from running PLACE offline, and 3) a 1.5-order turbulent kinetic energy (TKE) turbulence boundary layer. The code without changes, defined as the control code, uses the most widely applied land surface, soil initialization, and boundary layer options found in the current MM5 community code. As an initial test of these modifications, a case was chosen in which they should have their greatest effect: conditions where heterogeneous surface forcing dominates over dynamic processes. The case chosen is one with widespread summertime moist convection, during the Convection and Precipitation Electrification Experiment (CaPE) in the middle of the Florida peninsula. Of the eight runs, the code with all three changes (labeled TKE-PLACE) demonstrates the best overall skill in terms of biases of the surface variables, rainfall, and percent and root-mean-square error of cloud cover fraction for this case. An early, isolated convective storm that formed near the east coast, at the downwind edge of a region of anomalous wet soil, and within the dense cluster of CaPE mesoscale observation stations, is correctly simulated only by TKE-PLACE. It does not develop in any of the other seven runs. A factor separation analysis shows that a successful simulation requires the inclusion of the more sophisticated land surface model, realistic initial soil moisture and temperature, and the higher-order closure of the planetary boundary layer (PBL) in order to better represent the effect of joint and synergistic (nonlinear) contributions from the land surface and PBL on the moist convection.

1. Introduction

The evolution of Florida convection has been studied by numerous researchers (e.g., Byers and Rodebush 1948; Pielke 1974; Watson and Blanchard 1984; Nicholls et al. 1991; Boybeyi and Raman 1992; Kingsmill 1995; Atkins et al. 1995; Xu et al. 1996; Pielke et al. 1999). Blanchard and Lopez (1985) found basic recurring patterns, depending upon thermodynamic properties and changes in the prevailing upper-atmosphere wind. According to them, convection on any particular day over southern Florida is the result of complex interaction of many scales ranging from the global circulation (the Atlantic subtropical high pressure), the synoptic scale (waves and fronts), the peninsular scale (sea and lake breezes), and the local scale (heterogeneous soil/vegetation and cloud interactions).

Soil moisture distribution has been shown to affect dynamically driven circulations (Pielke et al. 1997) and landsacpe-forced circulations (e.g., Pielke et al. 1991; Avissar and Chen 1993; Mahrt et al. 1994). Chen and Wang (1995) found that clouds and rain can modify the surface thermal field of Hawaii, resulting in changes in the timing of wind shifts from downslope to upslope in the early morning. In addition, Lyons et al. (1995) found that soil moisture significantly affected the intensity of

Corresponding author address: Dr. Peter J. Wetzel, Mesoscale Atmospheric Processes Branch, Code 912, NASA Goddard Space Flight Center, Greenbelt, MD 20771.
E-mail: wetzel@elena.gsfc.nasa.gov

a Lake Michigan breeze. Shaw et al. (1997) showed the use of realistic heterogeneous soil moisture and vegetation may be necessary for the accurate prediction of dryline formation and morphology.

Here, the Pennsylvania State University–National Center for Atmospheric Research (PSU–NCAR) fifth generation Mesoscale Model (MM5) (Dudhia 1993; Grell et al. 1994) is configured to take advantage of two strongly interdependent, state-of-the-art advances in lower-boundary parameterization: a soil–vegetation–atmosphere interaction model and an improved model of turbulence processes. The land model is the Parameterization for Land–Atmosphere Convective Exchange (PLACE; Wetzel and Boone 1995), and the turbulence parameterization is an advanced turbulent kinetic energy scheme (TKE; Stauffer et al. 1999; Shafran et al. 2000). Performance of these model improvements, hereafter referred to as MM5 TKE-PLACE, is systematically tested using a matrix of simulations of the evolution of Florida summer moist convection on 27 July 1991, during the Convection and Precipitation Electrification Experiment (CaPE).

In section 2, we describe the model and methodologies for initializing the land surface soil and temperature fields. The experimental design is also detailed in section 2, then a brief synopsis of the case day is presented in section 3. Results of eight model simulations, systematically testing individual and combined changes to the control code, are presented in section 4. Sensitivity tests investigate the importance of the new boundary layer and land parameterizations, along with the impact of case-specific soil moisture and temperature initialization. A summary and conclusions are presented in section 5.

2. Method

a. MM5 modeling system

The PSU–NCAR mesoscale model, MM5, is configured here with two nested grids with horizontal resolutions of 15 and 5 km (the inner nest is shown in Fig. 1). The time step for the coarse grid was 45 s; it was 15 s on the fine grid. The two grids are time dependent and two-way interactive, and are centered over the Florida peninsula. There are 23 terrain-following sigma layers in the vertical, the lowest computational layer was about 40 m above the ground, and the highest resolution was in the lower troposphere. Explicit predictive equations are used for grid-resolved cloud water, rainwater, and ice (Grell et al. 1994) on both grids. A subgrid-scale moist convection parameterization (Kain and Fritsch 1990) is also used on the 15-km coarse grid mesh.

The control boundary layer scheme used here is the high-resolution scheme of Blackadar (hereafter called HIR; Zhang and Anthes 1982; Grell et al. 1994), which uses a local first-order closure during neutral and stable conditions and a nonlocal first-order closure during unstable (free convection) conditions. Although the medium-range forecast (MRF) boundary layer (Hong and Pan 1996) is becoming widely used in the current versions of MM5, it is not chosen as the control in this study because 1) it produces generally similar results to the Blackadar scheme (J. Dudhia 1999, personal communication), and 2) it appears in relatively fewer peer-reviewed MM5 studies to date.

The alternate scheme used in this study to represent turbulence processes is a 1.5-order TKE predicting scheme (Gayno 1994; Stauffer et al. 1999; Shafran et al. 2000). This higher-order scheme uses a prognostic equation to compute the local TKE profiles from which the model derives the eddy mixing coefficients used in the vertical diffusion of all mixing variables through the entire atmosphere. Therefore this scheme is not merely a planetary boundary layer (PBL) scheme but a general representation of turbulence, within cloud as well as in clear air. Vertical mixing is performed with liquid water potential temperature and total water mixing ratio due to their conservative properties during phase changes. If ice processes are active, ice–water liquid potential temperature is used, and an additional mixing variable for the cloud ice is added to the turbulence parameterization (Stauffer et al. 1999). The turbulence scheme used in this work is hereafter referred to as TKE, and is tested here coupled to both the control (SLAB) and the newly introduced (PLACE) land surface scheme.

The control land surface scheme uses a two layer force-restore method to compute the ground temperature as a function of the soil and vegetation characteristics defined by a lookup table. The surface physical characteristics include albedo, roughness length, emissivity, thermal inertia, and soil moisture availability. The ground temperature responds to surface radiation fluxes that vary in time; however, other surface characteristics, notably soil moisture, are held fixed in time.

The newly introduced land scheme, PLACE, represents soil and surface hydrology in considerably more detail. It allows soil moisture to change with time, as it interacts with evaporation, rainfall, infiltration, runoff, and soil water drainage to bedrock. The soil component of PLACE has five model layers for soil moisture plus two surface water storage reservoirs, and seven model layers for soil temperature. The vegetation component is represented by a single biomass layer that accounts for vegetation type, leaf area index, fractional cover, heat capacity, etc. Vegetation responds to the changing soil moisture and atmospheric environment via formulations for stomatal resistance and plant internal water flow. PLACE is also capable of explicitly representing subgrid surface heterogeneity through a mosaic of as many as 12 surface types. Further, statistically represented soil heterogeneity may be included within each subgrid ''mosaic tile'' (Boone and Wetzel 1996, 1999). The PLACE calculations are performed once every 3 min in the model for computational efficiency.

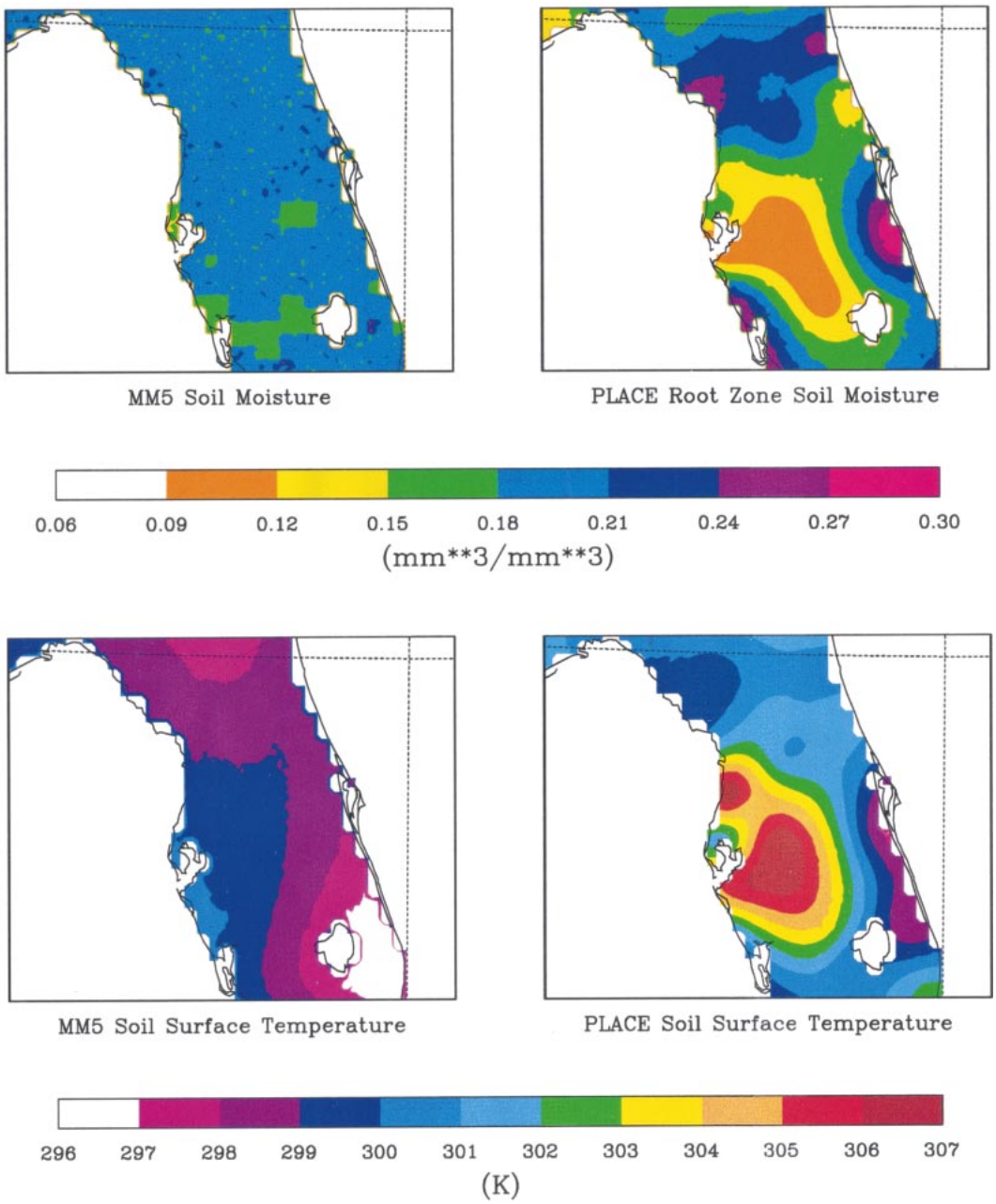

FIG. 1. MM5 Model preprocessor provided soil moisture (top left) and soil temperature (bottom left). Offline simulations of the PLACE model produced soil moisture and soil temperature fields, shown in plots, respectively, at top right and bottom right. The time was 0000 UTC 27 Jul 1991. Lake Okeechobee is shown at lower right corner of the domain shown. Note that the domain is assumed to contain no grid cells dominated by permanent wetlands. All soils are assumed to be well drained to at least 1-m depth.

b. Experimental design

Beside the incorporation of two major blocks of code within MM5, as discussed above, a third major change is tested: inclusion of case-specific initialization of soil moisture and temperature. A matrix of all eight possible permutations of changed and control runs are performed. Table 1 presents the naming convention for the eight simulations. The Blackadar high-resolution PBL is denoted ''HIR'' and the TKE turbulence scheme is denoted ''TKE.'' Following the hyphen, ''SLAB'' indicates the use of the force-restore land surface scheme and ''PLACE'' denotes the use of the PLACE land surface model. Finally, a ''0'' suffix to the experiment name denotes the use of the soil moisture based on climatology and soil temperature based on a temporal mean of the surface air temperature, both provided by the control

TABLE 1. Description of simulations discussed in the text. SLAB is the control, two-layer soil model. PLACE is a multilayer soil and vegetation land surface model. The ''0'' indicates that the control (climatology) soil temperature and moisture fields were used to initialize either land surface model. HIR is a first-order closure, high-resolution (Blackadar) boundary layer model, while TKE is a 1.5-order, turbulent kinetic energy scheme used in calculating boundary layer and cloud subgrid-scale fluxes. The moisture availability parameter required by SLAB is converted from volumetric soil moisture, m, by subtracting the wilting point value (m_{wilt}) and then normalizing the result by (dividing by) the difference between the field capacity and the wilting point ($m_{fc} - m_{wilt}$).

Acronym	Description
HIR-SLAB 0	Control model
HIR-SLAB	Soil fields from PLACE offline simulation
HIR-PLACE 0	PLACE land model replaces SLAB
HIR-PLACE	PLACE land model and soil fields from PLACE offline
TKE-SLAB 0	TKE boundary layer model replaces HIR
TKE-SLAB	TKE boundary layer, PLACE offline soil initialization
TKE-PLACE 0	TKE and PLACE models replace HIR and SLAB
TKE-PLACE	TKE and PLACE models with PLACE offline soil fields

MM5 preprocessor. No suffix ''0'' indicates use of offline PLACE-derived soil moisture and temperature fields.

The control MM5 preprocessor provides values of soil moisture availability based on climatology that do not change during the model run. The control code SLAB scheme does not attempt to update soil moisture based on precipitation, evapotranspiration, etc. Recent studies have demonstrated the importance of correct initialization of, and feedbacks to, soil moisture on the formation of convection (Chang and Wetzel 1991; Lynn et al. 1998). For this study, the alternate soil initialization is provided by running PLACE offline, forced by observations prior to the case date. Wind, precipitation, temperature and moisture fields from the National Climatic Data Center (NCDC) and from the CaPE Portable Automated Mesonet (PAM) observations were used. Figure 1 shows the initial soil moisture and temperature fields. These were obtained at the 30 observation data points where forcing data were available, then interpolated to the model nested grid using a linear interpolation technique. This was also done on the surrounding coarse grid, but these results were not shown. For comparison, Fig. 1 also shows the soil moisture and temperature fields obtained from the (control) MM5 preprocessor (after converting from the MM5 soil moisture availability to volumetric soil moisture). Since the control land surface scheme uses the top soil layer temperature and moisture, these fields are shown for them in Fig. 1. However, the soil moisture in the upper root zone layer (1–10 cm) is shown for PLACE, since this affects the latent heat flux from vegetation (which is usually larger than that from the soil surface). Note that the PLACE-derived fields contain two regions of relatively dry soil with warm soil temperatures. There are also two maxima in soil moisture, corresponding to relatively cool initial soil temperatures.

The MM5 is initialized at 0000 UTC 27 July 1991, and integrated for 24 h until 0000 UTC 28 July 1991. Initial and lateral boundary conditions are specified on the 15-km coarse grid mesh via an objective analysis performed at 12-h intervals, using conventional data and National Centers for Environmental Prediction (NCEP) spectral analyses. The vegetation cover is initialized using the standard MM5 preprocessor in which the surface characteristics and associated parameters are specified as a function of cover type via a lookup table. The PLACE vegetation model requires additional parameters that the control preprocessor does not provide. For this reason, data from the International Satellite Land Surface Climatology Project (ISLSCP; Meeson et al. 1995) were used to obtain values of fractional vegetation cover and leaf area index, albedo, and surface roughness. To do so, we equate ISLSCP vegetation types and soil types with land types given by the MM5 preprocessor. Variables such as thermal conductivity and emissivity of the ISLSCP-provided types were derived from values commonly available in the literature. It must be noted that all eight simulations discussed herein use the same vegetation and soil type distributions. All associated initial conditions describing the land surface are identical in all runs with the lone exceptions being the soil moisture and temperature.

The goal of this study is to use a single case to begin evaluating whether there is added value by coupling the PLACE and TKE schemes to MM5. We will use both subjective (qualitative) and objective (statistical) analysis, a methodology that is commonly applied to evaluating mesoscale model simulations (e.g., Pielke 1984, Shaw et al. 1997).

3. Case description

The case of 27 July 1991 from the CaPE experiment dominated by a weak synoptic-scale wave approaching Florida on a prevailing westerly wind. The wave generally enhanced convection that otherwise responded fairly typically to the west wind conditions (Blanchard and Lopez 1985). Convective clouds formed first around 1600 UTC near the west coast, and then later, by 1800 UTC along the east coast. At 1800 UTC the leading edge of an irregular formation of convective storms had already reached the central peninsula, and, typical of days with westerly flow, the weaker east coast convection had made relatively little progress westward. Only one significant east coast convection cell had developed by 1800 UTC (see Fig. 2). Its isolation and location are significant because it not only formed within the dense network of surface stations put in place for the CaPE experiment, but it also formed at the leeward (northwest)

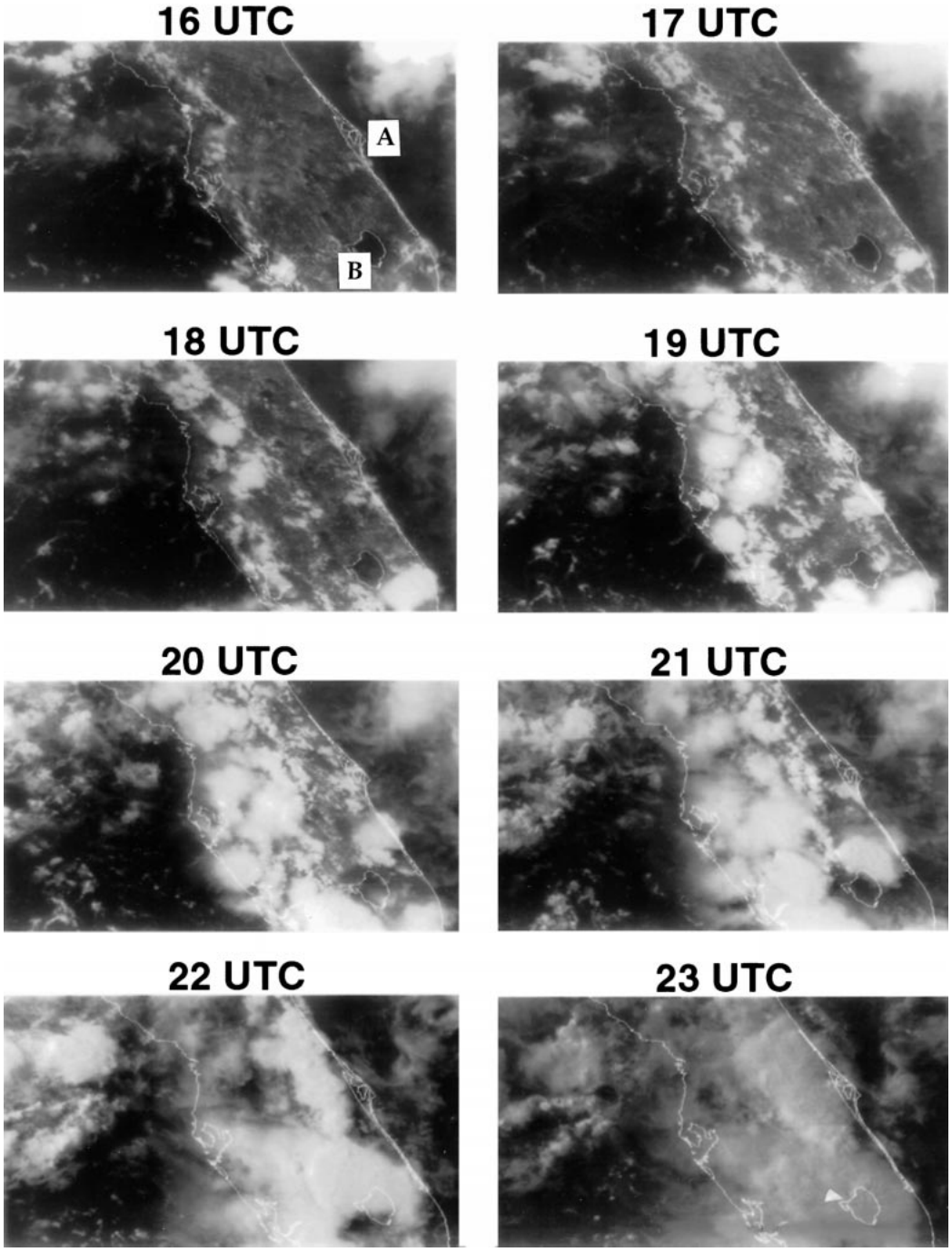

FIG. 2. Visible satellite pictures of the central Florida peninsula, encompassing the nested domain used in the model simulations. Specific locations referred to in the text are identified with letters on the 1600 UTC image. Point A is Cape Canaveral, Point B is Lake Okeechobee.

boundary of the anomalous wet soil region depicted in Fig. 1.

For detailed discussions of this case day, including radar observations, detailed surface analyses, budget studies, and analysis of physical processes, the reader is referred to three previous articles published in this journal. Fankhauser et al. (1995) and Halverson et al. (1996) also produced two-dimensional simulations of CaPE convective events. Wilson and Megenhardt (1997) documented the merger of the west coast convection lines with the east coast convergence zone, leading to intensified thunderstorm development. By 2000 UTC, an irregular band of thunderstorms dominated the western half of the peninsula and smaller convective clouds

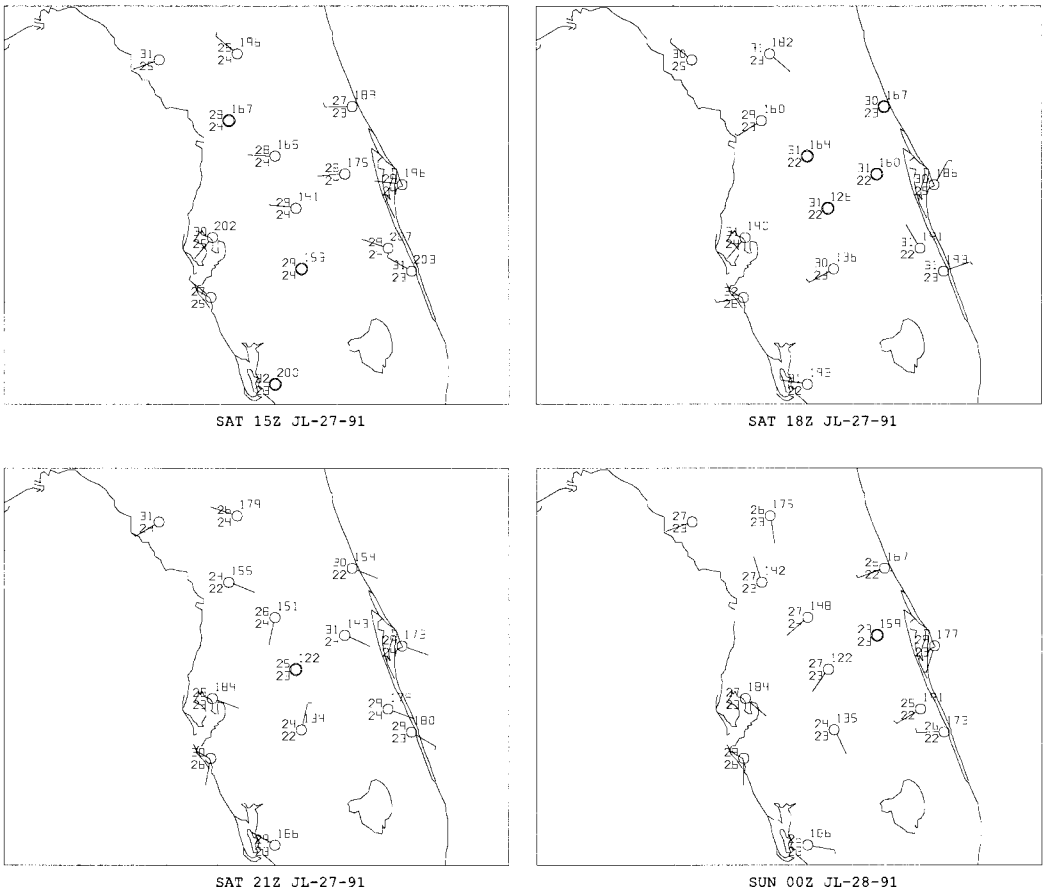

FIG. 3. Surface data obtained from PAM and National Weather Service reporting stations. Figures show pressure, temperature, dewpoint and wind on 27 Jul 1991 at 1500 UTC (top left), 1800 UTC (top right), 2100 UTC (bottom left), and 2400 UTC (bottom right). A tail on the station circle represents a surface wind of 5 m s^{-1}, while a barb on the tail indicates an additional 5 m s^{-1}.

and storms occurred just inland of the east coast (Fig. 2). Between 2000 and 2200 UTC, the separate identity of these two groups disappears into one large mass of clouds that dominates the eastern half of the peninsula by 2300 UTC.

Plotted in Fig. 3 are station observations of surface pressure (tenths of hPa with first two digits deleted), temperature (°C), dewpoint (°C), and wind (m s^{-1}), obtained from PAM sites and National Weather Service stations (14 data points). Surface pressure dropped quite substantially, between 1500 and 1800 UTC (1000–1300 LST), especially over the northern and central part of the peninsula, in association with an approaching synoptic-scale disturbance (J. Halverson 2000, personal communication; this is also evident in Fig. 2 by the cloud mass over the Gulf of Mexico in the northwestern corner of each satellite image). Note that in locations where the PLACE initialization indicates relatively dry soil in Fig. 1 (i.e., <0.18 mm^3 mm^{-3}), the average increase in temperature was 2 K, but in locations of moist soil, the average increase was about 1.1 K. Since evaporation over moist soil operates to keep surface temperature cooler, this observation provides indirect confirmation of the PLACE initialization.

Figure 4 shows accumulated rainfall on 27 July 1991, tabulated from NCDC and PAM sites, for the periods 1800–2100 UTC and 2100–2400 UTC. Each field was obtained after interpolating with a Barnes scheme (Barnes 1964). For 1800–2100 UTC, the western half of Florida received the most rainfall. In contrast, the 2100–2400 UTC accumulated rain was largest over south-central and eastern Florida. The rainfall maxima during each time period correspond well with the sequence of satellite pictures. Notice the relatively large magnitude of measured rainfall over a point in eastern Florida coincident with the earlier isolated convection (Fig. 2; 1700–1900 UTC) and with the maximum in soil moisture (Fig. 1, upper right panel). One station there reported 53.75 mm of rain within 1 h. Any remnant moist downwash (outflow) from the earlier convective storm could have combined with the already moist soil in this area to provide added moisture to the convection that approached from the west. Figure 3, at 2100 UTC, depicts the westward push of surface air in this region.

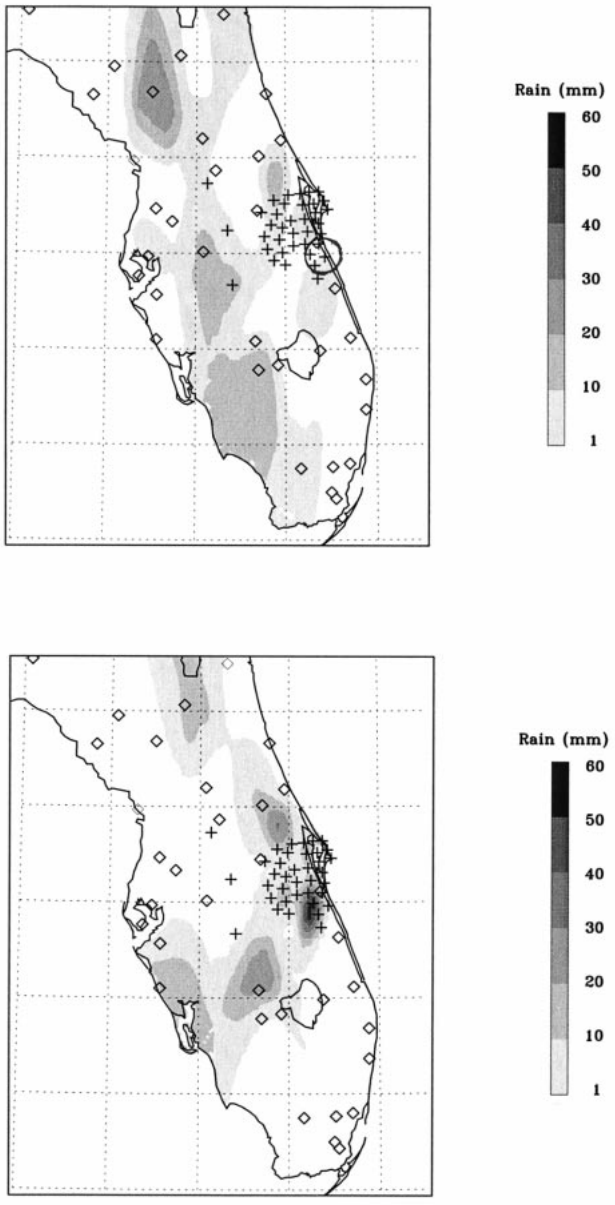

FIG. 4. Accumulated rainfall obtained from PAM sites (''+'' sign) and NCDC observing stations (diamond) on 27 Jul 1991 between 1800–2100 UTC (top) and 2100–2400 UTC (bottom). The analyses were produced using a Barnes interpolation. Four PAM stations in vicinity of the soil moisture maximum on the east coast (Fig. 1), which are analyzed in detail later in the paper, are circled in the top panel.

Hourly analyses of PAM network station data, not shown, suggest that the outflow from the earlier storm combined with the east coast sea breeze–like flow to produce a westward bulge of cool, moist air that met the storms approaching from the west. The storms are likely to have then processed this moisture and returned it eastward, dropping it near its presumed point of origin at the soil moisture maximum. Clearly a very complex chain of interactions over several hours occurred to produce this precipitation maximum. In order for a model to reproduce this multihour chain of events exactly as observed, every individual link in the chain would have to be modeled correctly. Unfortunately, none of the eight model simulations produced the resulting precipitation maximum near the location where it was observed. But, as will be discussed in the next section, the TKE-PLACE run is the only one of the eight to have correctly predicted the first link in the chain: the isolated east coast convective cell that formed at the boundary of the soil moisture maximum.

4. Results

a. MM5 TKE-PLACE and MM5 HIR-SLAB 0

In this section, we apply all available observational data to the validation of the eight model results. We place special emphasis on the comparison between TKE-PLACE, which contains the package of all three modifications (the intended mode of running the model for future studies), and HIR-SLAB 0, which contains none of these (the package most commonly used in past studies). Due to constraints of space, individual and ensemble intercomparisons from all eight models are summarized in a series of tables. This section concludes with a detailed look at the simulation of the isolated east coast storm which formed at the boundary of a small region of anomalous moist soil. The following section further examines results of all eight model runs (Table 1), using a ''factor separation'' technique to explore in detail the individual role of each of the three model changes as well as the role of interactions between any two, and among all three, of the changes.

This study used four sets of observations to evaluate the model results: (i) the surface fluxes at observational sites (two points, both on Cape Canaveral); (ii) the surface meteorological observations (37 points, most heavily concentrated on the eastern side of the peninsula, see the ''+'' symbols in Fig. 4); (iii) area-averaged rainfall (63 points, all symbols in Fig. 4); and (iv) fractional cloud cover [satellite data (Fig. 2) with uniform, almost complete, high spatial resolution coverage of the entire domain].

Figure 5 shows the sensible heat fluxes obtained with HIR-SLAB 0 and TKE-PLACE at 1500 UTC, for the nested domain. Differences over ocean areas are indicative of the divergent solution for surface wind between the two runs. Over land HIR-SLAB 0 had a relatively uniform distribution of sensible and latent heat fluxes. In contrast, areas that had relatively dry ground in TKE-PLACE produced strong sensible heating. As noted by Shaw et al. (1997), the partitioning of the net radiation balance at the surface responds most strongly to the soil moisture distribution because the equilibrium timescale for soil moisture is longer than that for soil temperature. Because the surface fluxes were very small by sunrise (about 12 h after the simulation began), the TKE-

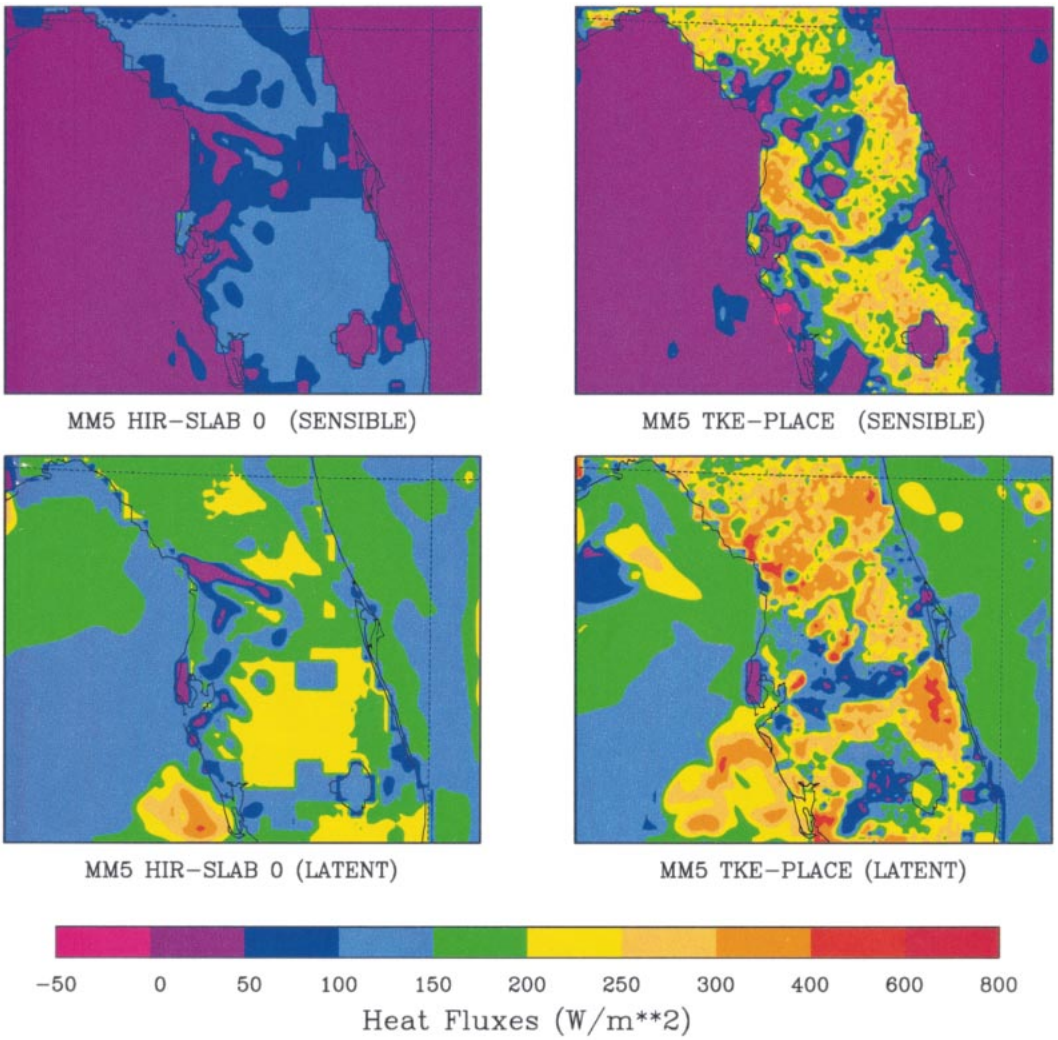

FIG. 5. Horizontal distributions of surface sensible heat flux (top) and latent heat flux (bottom), obtained by HIR-SLAB 0 and TKE-PLACE model runs on 27 Jul at 1500 UTC. Note that there is a direct correspondence between the four panels shown here and those of Fig. 1. That is, the HIR-SLAB 0 fluxes were obtained using its customary initialization (at left), and the TKE-PLACE fluxes were obtained using its associated PLACE offline initialization (at right).

PLACE initial surface temperature, which is shown in Fig. 1, had likely very little impact on the development of daytime surface fluxes.

The modeled fluxes were compared to the observed surface energy budget (two data points on Cape Canaveral along the east coast). Given the availability of flux data only over the cape, in close proximity to the ocean, an intercomparison with the model is felt to be anecdotal in nature, although it nevertheless is instructive. We compare the observations with data averaged over a 25-km strip of model grid cells centered along the cape (the relatively coarse, 10-min MM5 land use data used here makes collocated comparison difficult since much of the Cape is treated as water by the model; see Fig. 1). Results are shown in Fig. 6. TKE-PLACE produces more realistic sensible heat fluxes than HIR-SLAB 0, while both runs produce similar latent heat flux and both agree reasonably well with the observed incoming solar radiation flux. However, the observed sensible heat flux is considerably larger than modeled. The differences between the MM5 simulations and observations are very likely caused by the soil characteristics found on the cape. The soil there is virtually pure sand that has very low thermal conductivity. The modeled soils (identical in all runs) represent the mainland soil types that have considerably larger conductivity. The sand at the observation sites results in a much higher surface temperature. At the same time, easterly winds (Fig. 3) continuously advect cool maritime air over this warm surface. This combination leads to a much larger sensible heat flux. The low thermal conductivity of the sand allows little exchange of heat into the ground. On

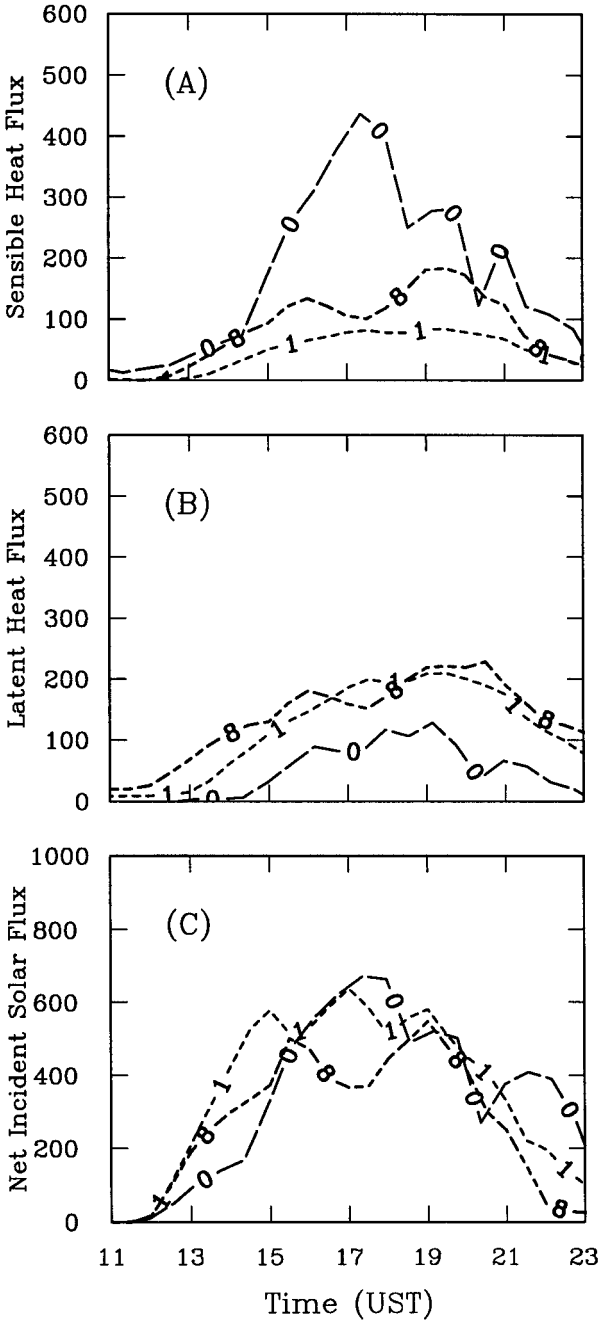

FIG. 6. Time dependence of surface sensible heat flux, surface latent heat flux, and surface net radiation obtained from observations (''0''), HIR-SLAB 0 (''1''), and TKE-PLACE (''8''). The units for each are W m^{-2}. There were two flux observation points located on Cape Canaveral; they were averaged to produce these plots. The model data were averaged over areas corresponding roughly to the size of the cape.

the other hand, the ground heat flux in the model simulations (not shown) is larger than the observations, and the colder modeled surface temperatures that result enhance the differences in sensible heat flux.

The region around the cape was dominated by east winds until late in the day (Fig. 3). The shallow layer of cool maritime air over the surface is a condition that the HIR boundary layer model has difficulty simulating. The HIR model contains a software switch between shallower mechanically forced unstable boundary layer and the daytime free convection regime that dominates in deeper boundary layers inland. As with any case of flow from cold water to sun-heated land, the actual daytime boundary layer over the flux sites is one of a rapid transition from mechanically forced convection (near-neutral lapse rate) to a very vigorous but shallow free convection boundary layer. The HIR model underpredicted sensible heat because, given the vertical resolution of these simulations, HIR was unable to represent the free convection that actually existed. The TKE model, on the other hand, allows the PBL to develop according to the predicted turbulence profile, which represents free convective (buoyancy) and mechanical (shear) forcings simultaneously, rather than in different regimes based on the magnitude of the surface fluxes. This appears to have worked to its advantage at this transitional site. We reiterate, however, that comparison of the surface energy budget at just two stations in one small subset of the model domain cannot be considered a comprehensive test of the models' performance.

Table 2 summarizes the performance of all eight model runs at predicting surface meteorology at the 37 PAM stations at a time just before deep convection began (1600 UTC), and for the entire 12-h period from 1200 to 2400 UTC. The table presents raw biases (average of point differences between model and observation) for five meteorological parameters and then ranks each run based on the overall performance of each run at simulating all five variables. Three methods of ranking the models (from a rank of 1 for the best performing model to 8 for the worst) were applied. In the first method, the distributions of all five variables were normalized so their deviations from observations were of equal weight, while in the second method, only the mean of each variable was normalized and used to scale the absolute value of intermodel variability. The third method ranked the individual variables separately and then these ranks were averaged. All three methods produced reasonably similar results. Presented in Table 2 is the arithmetic average of the resulting ranks from all three methods. Note that TKE-PLACE did marginally better than HIR SLAB 0, although four other runs outperformed TKE-PLACE in this overall ranking for the total 12-h study period.

In order to further evaluate this rather ambiguous result, ensemble results are presented at the bottom of Table 2. Here four runs, with and without a particular model change, are combined. The ranking associated with each of these ensembles is an average of the rankings from the individual runs rescaled to the 1–8 scale {since the average ranking that the four best runs of eight can have is 2.5 [(1 + 2 + 3 + 4)/4] and the worst ranking is 6.5}. These ensemble results show that the

TABLE 2. Biases and rankings for meteorological data at 37 PAM observational sites, all concentrated on the eastern side of the peninsula (see Fig. 4, ''+'' symbols). The first eight rows show results at one time only, 1600 UTC. The second eight rows show the average results for the 12-h period 1200–2400 UTC 27 Jul 1991. The last six rows each represent ensemble averages of four runs that have the single labeled model feature in common (the ''1'' refers to the simulations with PLACE offline boundary conditions). Rankings are a synthesis of the model performance for all five meteorological variables, with possible ranks for individual rows ranging from 1 (best possible) to 8 (worst possible). See text for further details.

Acronym	Pressure (hPa)	Temp. (K)	Dew point (K)	Wind speed (m s^{-1})	Wind direction	Rank
1600 UTC						
HIR-SLAB 0	0.04	−3.18	−1.75	−1.38	111.81	7.33
HIR-SLAB	−0.20	−2.45	−1.86	−1.06	137.61	7.67
HIR-PLACE 0	−0.11	−2.56	−1.44	−0.63	140.23	5.67
HIR-PLACE	−0.39	−2.47	−0.85	−0.04	130.49	5.33
TKE-SLAB 0	0.11	−2.84	−0.79	1.04	18.06	3.67
TKE-SLAB	−0.16	−2.24	−1.30	0.92	24.37	2.33
TKE-PLACE 0	−0.13	−2.26	−0.38	−0.40	46.92	2.00
TKE-PLACE	−0.19	−2.47	0.02	0.13	73.50	2.00
1200–2400 UTC						
HIR-SLAB 0	0.58	−1.83	−1.05	0.68	68.80	5.83
HIR-SLAB	0.14	−1.04	−0.87	1.45	78.15	3.83
HIR-PLACE 0	0.31	−1.49	−0.68	0.26	71.86	1.67
HIR-PLACE	−0.01	−1.19	−0.26	1.17	74.86	1.13
TKE-SLAB 0	0.70	−2.56	−0.78	2.19	57.17	7.67
TKE-SLAB	0.53	−2.10	−1.01	2.16	63.68	7.17
TKE-PLACE 0	0.64	−2.73	−0.18	0.75	68.21	3.33
TKE-PLACE	0.54	−2.73	−0.09	1.19	73.68	5.17
PLACE	0.37	−2.03	−0.30	0.84	72.15	1.66
SLAB	0.49	−1.88	−0.93	1.62	66.95	7.34
TKE	0.60	−2.53	−0.52	1.57	65.69	6.83
HIR	0.26	−1.39	−0.71	0.89	73.42	2.17
1	0.30	−1.76	−0.56	1.49	72.59	4.28
0	0.56	−2.15	−0.67	0.97	66.51	4.72

PLACE land scheme produced a major improvement in the model performance compared to the SLAB scheme, and that the four runs with PLACE offline initialization produced slightly better results than the climatology initialization. However, the more sophisticated TKE boundary layer scheme actually produced greater surface meteorology biases than the simple HIR scheme over these 37 PAM sites. These sites are all concentrated over the eastern side of the peninsula. The results could be quite different on the western half of the peninsula, where deep convection developed early and was more significant through the early part of the day. Most convection reaches the east late in the day after model errors have had an opportunity to multiply (slight errors in modeling initiation of the first convection can lead to mislocated and mistimed outflow boundaries, leading to greater errors in secondary convection formation, etc.). The possibility that error multiplication led to the apparent poor performance of the TKE runs can be explored further by comparing the 1600 UTC biases with the overall 12-h average biases.

In Table 2, at 1600 UTC, the biases suggest that the addition of each of the three model changes makes a positive contribution to improving the model performance. The only exception to this is the surface pressure, which seems not to be systematically affected. However, for the 12-h period as a whole, the changes actually appear to have an overall inconclusive effect on most variables, but to notably worsen the temperature bias. In particular, the four TKE runs are 1–1.5 K colder than the four HIR runs. It is also apparent that an underlying cold bias exists in all model runs. The most probable causes for an overall cold bias are 1) a tendency of the model to underpredict the transmission of solar radiation by clouds, 2) a too-moist soil moisture initialization, 3) incorrect representation of the relationship between surface fluxes and the shape of the temperature profile between the surface and the lowest model layer, 4) a too-dry initial relative humidity field over the peninsula that could cause excessive radiative cooling at night and/or greater evaporative cooling and stronger outflow boundary winds during the day, or 5) an excessive soil thermal conductivity, as discussed above. Because the change from HIR to the TKE boundary layer shows the most significant effect on temperature bias, and because the TKE runs systematically produce very much more cloud than the HIR runs (see below), it seems most likely that the MM5 cloud transmittance functions caused too little solar radiation to reach the surface. This problem has been reported by other researchers as well; and the cloud shortwave radiation scheme in the most recent version of MM5 (version 3) has been modified to reduce the cloud effects on shortwave radiation, particularly from cirrus clouds, and to a lesser extent from rainwater (J. Dudhia 2000, personal communication). There is also some evidence

TABLE 3. Observed, modeled rainfall and rankings for 1200–2400 UTC. The second column is a simple average at observation sites. The third column is a composite of area averages. For this column the peninsula was divided into four equal area geographic quadrants over which rainfall was averaged (NW, 6 stations; NE, 27 stations; SW, 7 stations; SE, 24 stations). As in Table 2, the last six rows represent four-run ensemble averages. Rankings for individual runs are average ranks for the two methods. Rankings for the four run composites are averaged then rescaled, as in Table 2.

Acronym	Stations (mm)	Areas (mm)	Ranking
Observations	9.17	8.96	—
HIR-SLAB 0	2.06	2.17	8.0
HIR-SLAB	2.30	2.83	6.0
HIR-PLACE 0	2.71	2.80	6.0
HIR-PLACE	5.13	3.77	4.0
TKE-SLAB 0	9.57	9.31	1.5
TKE-SLAB	12.98	14.48	3.5
TKE-PLACE 0	13.51	15.21	5.5
TKE-PLACE	10.25	8.96	1.5
PLACE	7.90	7.68	4.06
SLAB	6.73	7.20	4.94
TKE	11.58	11.99	1.88
HIR	3.05	2.89	7.13
1	7.66	7.51	3.19
0	6.96	7.37	5.81

for the excessive cloud effect from the net shortwave flux measurements shown on Fig. 6c for late in the day.

A comparison of model predicted rainfall with observations (Table 3) showed that TKE-PLACE's station average precipitation was 10.25 mm compared to 9.17 mm observed, and its area average was 8.96 mm, which was identical to the observed value. The ranking shows TKE-PLACE tied for the best ranking, while HIR-SLAB 0 had the worst. The results summarizing the impact of each of the changes show that the boundary layer scheme has by far the largest effect on the rainfall. The ensemble of four runs that used the TKE boundary layer scheme produced much more rainfall than the four runs that used the HIR scheme. This is most likely a result of the lack of the use of a cumulus parameterization in the 5-km resolution interior nest. The new TKE scheme is designed to be able to effectively link boundary layer turbulence with that within the resolved cloud, and to seamlessly transport water substance between the subcloud layer and the cloud (e.g., Stauffer and Seaman 1999). The HIR scheme computes a boundary layer depth based on virtual potential temperature, considering dry adiabatic processes alone, so it fails to properly treat fluxes through cloud base. Therefore any resolved cloud that forms above its calculated boundary layer top must entirely generate its own turbulence ''from scratch'' after it forms. Only weak background diffusion is applied in the Blackadar scheme above its diagnosed PBL height. This unnatural restriction may suppress cloud and rain development in HIR runs when no cumulus parameterization is used.

TKE-PLACE did much better than HIR-SLAB 0 in simulating the observed cloud fraction. Because cloud cover is the only observed quantity with high spatial and temporal resolution over the entire modeled domain, we consider analysis of this variable to be critical for evaluating model performance in this case. Cloud fraction, as observed by satellite (Fig. 2), was digitally compared with the model predicted equivalent. However, first we examine the qualitative results. Figures 7 and 8 show modeled cloud condensate from the HIR-SLAB 0 and TKE-PLACE, respectively. Qualitatively comparing Figs. 7 and 8 with Fig. 2, TKE-PLACE appears to have produced a better simulation of the following cloud cover features: (i) convective cloud development early in the day, notably including that which occurred over the ocean; (ii) an irregular band of convective cells consolidating inland from the west coast and an isolated east coast storm, both apparently forming partially in response to sea-breeze circulations (not shown); (iii) correct west to east movement of the storms, although perhaps somewhat earlier/faster than observed; and (iv) the timing and location of convection near Lake Okeechobee, outlined in the lower-right portion of the figures. These features were not well simulated by HIR-SLAB 0.

Figure 9 shows a scatterplot of the quantitative comparison of observed versus modeled fractional cloud cover. The observed fractional cloud amount was obtained by simply identifying the appropriate brightness threshold, then counting pixels with cloud and dividing by total pixels within a specified subset of the domain. The modeled fractional cloud cover was determined by counting the number of model grid cells with cloud amount above a threshold value and dividing by the total number of grid cells. Since choosing the model threshold is more arbitrary, this calculation was done three times using different thresholds and the three results were averaged. The result, plotted in Fig. 9, shows that although the TKE-PLACE run has a slight negative cloud bias, it produced many more points within 25% of the observations than did HIR-SLAB 0. Note also that HIR-SLAB 0 had a very marked negative bias (see also Fig. 7). As discussed above, this is probably a result of the inadequate treatment of boundary layer to cloud transport when HIR is used without a cumulus parameterization in high-resolution simulations.

Table 4 summarizes the statistics for the scatterplot of Fig. 9, by showing the domain-averaged cloudiness and root-mean-square error. Two measures of root-mean-square error are shown in Table 4. The first indicates the model skill in obtaining the timing of the domain-averaged fractional cloudiness (RMS_1), while the latter indicates the model skill in obtaining the correct timing and location of cloud cover within eight subdomains of the peninsula (RMS_2). TKE-PLACE produced much better total cloud cover and much smaller values of RMS_1 and RMS_2 than did HIR-SLAB 0.

Finally, we examine the surface wind and temperature fields associated with the isolated east coast convective cell that formed at the upwind edge of a small area of anomalous moist soil (Figs. 1 and 3). This storm is

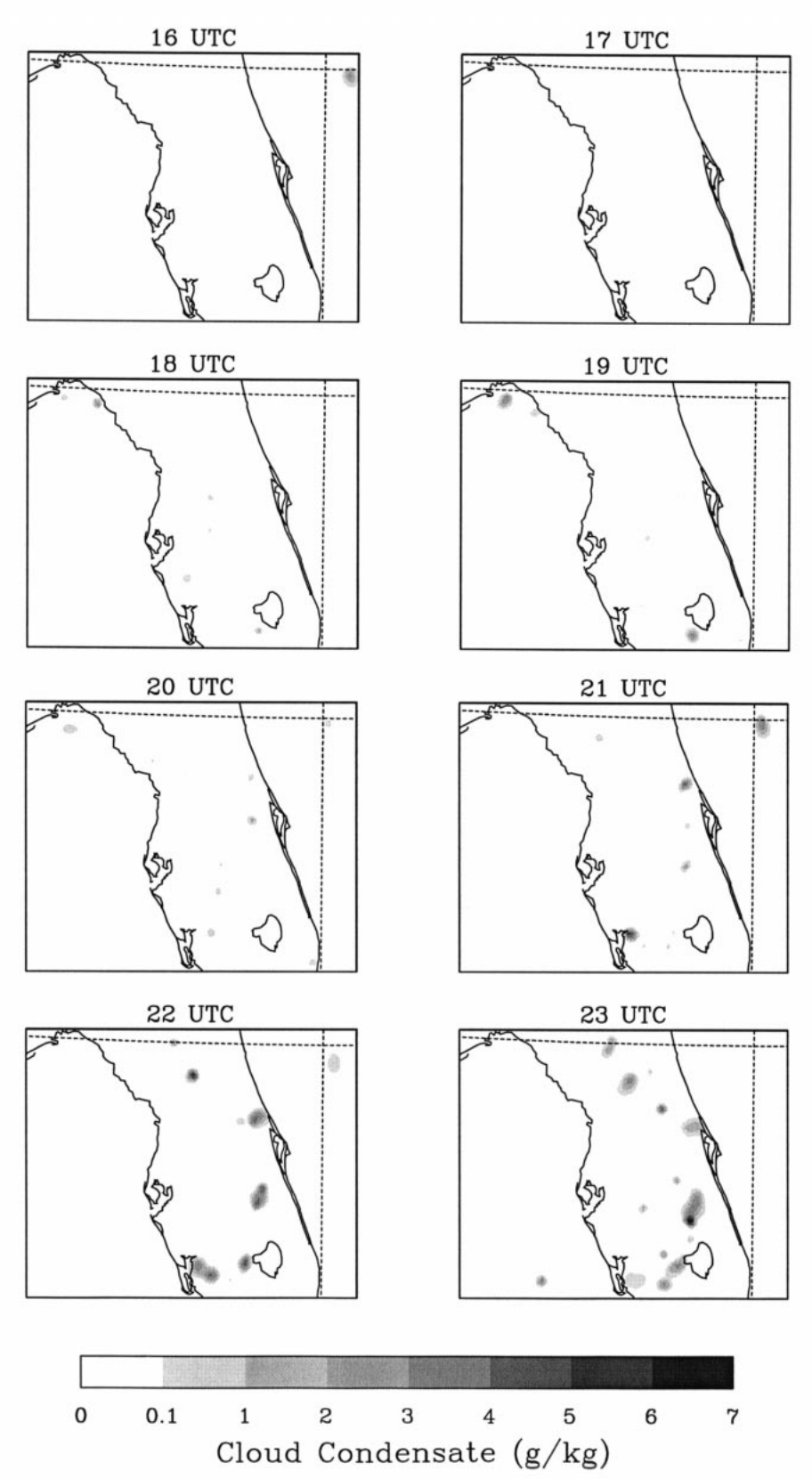

FIG. 7. A plot of vertically integrated cloud condensate over the layer 1–8 km above the surface for the HIR-SLAB 0 run, at the times shown in Fig. 2. A simple layer average was used to obtain these plots.

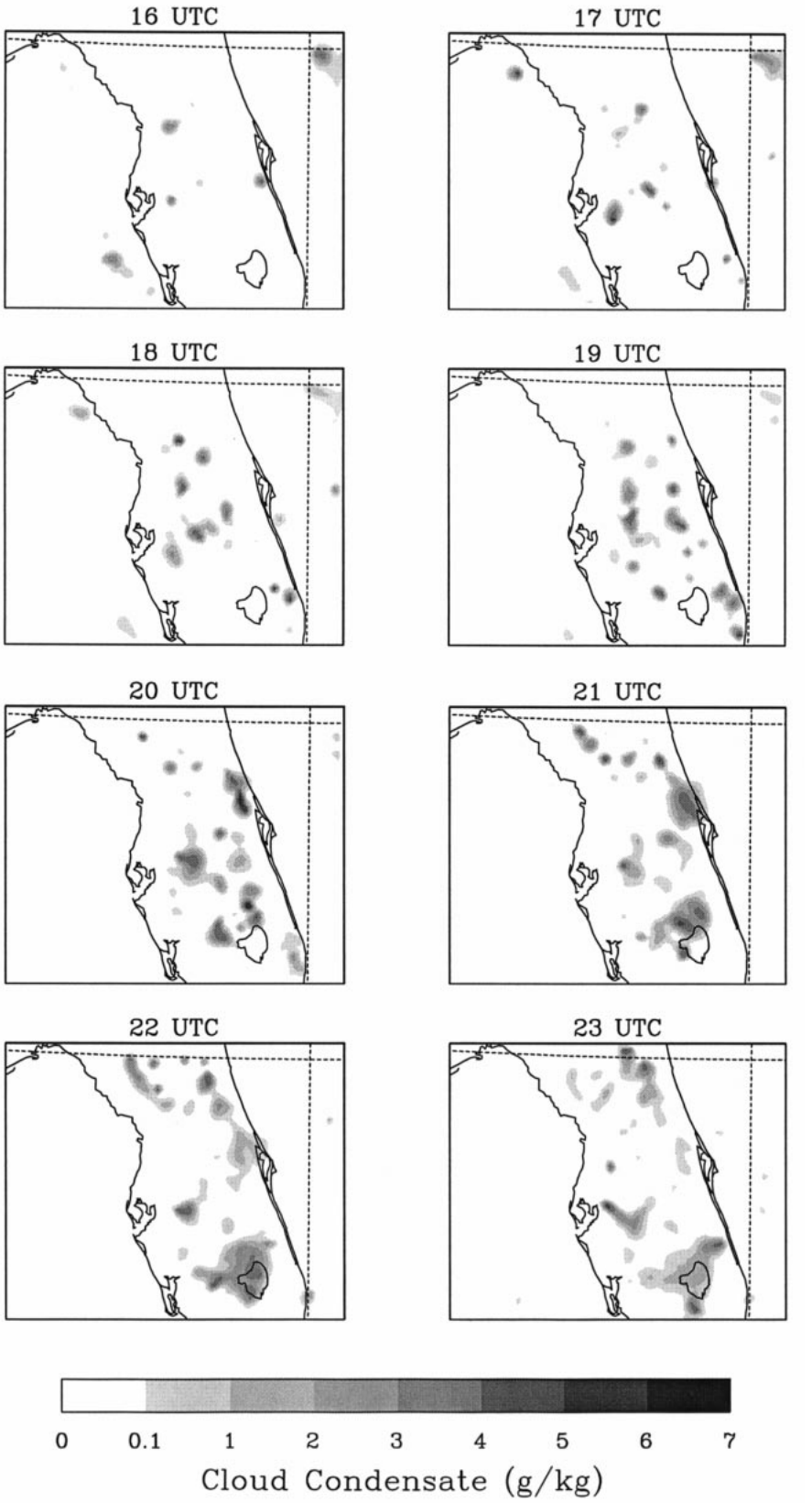

FIG. 8. Same as Fig. 7, but for the TKE-PLACE run.

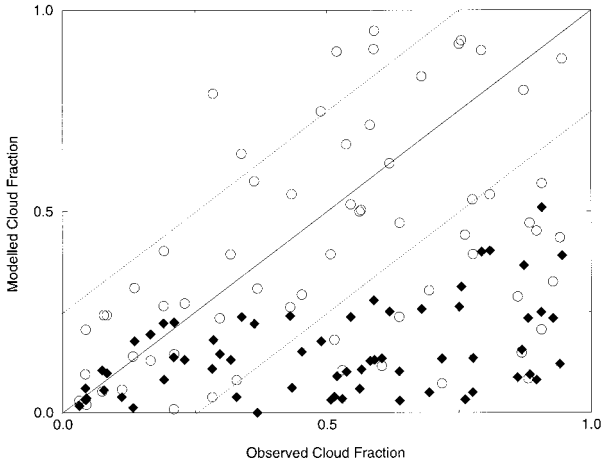

FIG. 9. A scatterplot of observed vs modeled fractional cloud cover for TKE-PLACE (circles) and HIR-SLAB 0 (diamonds). Data points falling along the solid line had no error. The dotted lines indicate the range of ±25% error. See Table 4 for a description of the method used to obtain fractional cloud cover from the observations and model output.

TABLE 4. Average fractional cloud amount for 1600–2300 UTC, obtained in each simulation, percent of modeled vs observed cloud amount, two estimates of root-mean-square error (rmse) of modeled vs observed fractional cloud amount, and average rankings (as in Table 2). The observed fractional cloud amount is obtained by applying a threshold brightness to each pixel of the digital images shown in Fig. 2. Modeled fractional cloud amount in each individual grid cell is similarly assumed to be either 0 or 1 based on a threshold value of 0–8 km averaged cloud water mixing ratio. For the model result, three different thresholds were applied, using 0.001, 0.01 and 0.1 g kg^{-1}. Results for the three thresholds were averaged to produce the numbers here. Rmse_1 is calculated from the total cloud amount over the entire peninsula, one value for each of the eight time periods of Fig. 2. This indicates the model skill in simulating the timing of the gross cloud amount. Rmse_2 attempts to evaluate model skill in both timing and location of cloud amount by comparing model and observed cloud amount in each of eight equal-area regions of the peninsula (NE corner, NE central, SE central, SE corner, NW corner, etc.). The last six rows are four-run ensemble averages, as in Table 2. The average observed fractional cloud cover for the 8-h period was 0.40.

Acronym	Fractional cloud cover	% of observed	rmse_1	rmse_2	Ranking
HIR-SLAB 0	0.12	31	0.40	0.44	8
HIR-SLAB	0.17	41	0.33	0.42	6
HIR-PLACE 0	0.15	38	0.37	0.43	7
HIR-PLACE	0.19	47	0.31	0.42	5
TKE-SLAB 0	0.21	51	0.27	0.35	4
TKE-SLAB	0.23	58	0.24	0.34	3
TKE-PLACE 0	0.28	68	0.19	0.33	2
TKE-PLACE	0.32	80	0.14	0.32	1
PLACE	0.24	58	0.25	0.38	3.18
SLAB	0.18	45	0.31	0.39	5.81
TKE	0.26	64	0.21	0.34	1.00
HIR	0.16	39	0.35	0.43	8.00
1	0.23	56	0.26	0.38	3.19
0	0.19	47	0.31	0.39	5.81

considered an important benchmark for four reasons. (i) It is isolated and formed early in the day, so it was responding to significant forcing mechanisms which are likely to be easier to reproduce by the model. Later convection is less likely to be modeled accurately because of multiplying errors in location and timing of storm outflow boundaries, surface cloud shading, and cooling by precipitation. (ii) It formed directly over a wet soil anomaly, which provides one of the possible triggering mechanisms, one which the TKE-PLACE model is expected to handle reasonably well. (iii) Of all eight MM5 simulations produced for this study, only TKE-PLACE developed this storm. It did not occur at all in any of the other seven runs. (iv) It may have played a role, as discussed earlier, in generating the heavy isolated precipitation event that occurred later in the day in the same location (Fig. 4b).

Comparing Figs. 7 and 8 with Fig. 2, one finds that a small cell of cloud and rain water occurs at 1600 UTC in the TKE-PLACE run (Fig. 8) that is exactly col1ocated with a very small, very isolated patch of clouds discernible at 1600 UTC in the satellite image (Fig. 2). No such cell developed in the HIR-SLAB 0 simulation (Fig. 7) or in any of the other runs not shown. By examining the rate of growth of this cloud on the satellite image, and by examining the hourly precipitation records (not shown), it is apparent that TKE-PLACE is about 1.5 h premature in developing this storm into a precipitating system. In the satellite imagery, it appears to develop deep convection between 1800 and 1900 UTC. Precipitation data show that it produced precipitation (at the available observation stations) beginning about 1700 UTC. However, by 1700 UTC in the TKE-PLACE run, the cloud and rainwater were already diminishing and moving eastward, indicating that the remaining liquid water was aloft and that the storm was dissipating.

Beside the soil moisture anomaly, a myriad of factors could have contributed to the formation of this storm, including any preexisting outflow boundaries, such as from the nocturnal convection seen over the ocean northeast of the cape, interactions with subgrid land use, and soil moisture discontinuities, etc. Similarly, a myriad of factors could cause the 1.5-h premature formation of the storm in TKE-PLACE. One cannot even rule out that the storm formed ''in the right place for the wrong reason.'' However, comparison between the model results and surface observations suggests that the model was responding accurately and in a physically realistic manner. We discuss this further next.

To evaluate the performance of TKE-PLACE in evolving the environment of this storm and its aftermath, we averaged four PAM station observations in the storm's vicinity and compare them with TKE-PLACE. Figure 10 depicts the *u* component (east–west) of the wind field as averaged from surface observations at the four stations and as modeled at ~40 m above ground level (AGL) by TKE-PLACE. Also shown on the figure

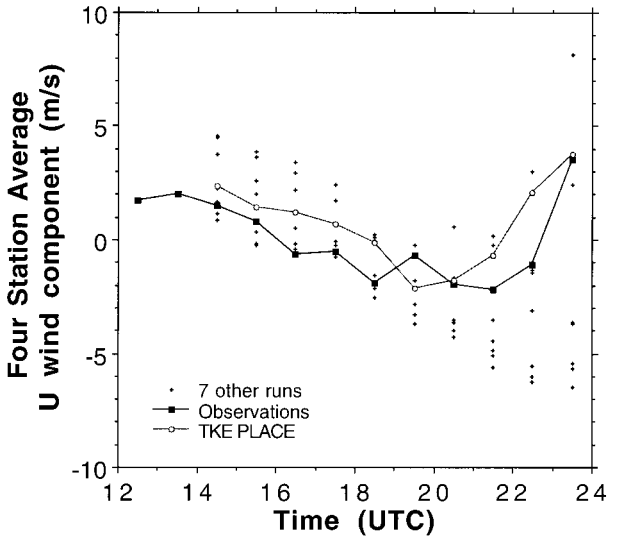

FIG. 10. Time series of the *u* component (east–west) of surface (or lowest model level) wind. Observations are the average of four stations in the vicinity of the soil moisture maximum (circled "+" station symbols on Fig. 4). Model results are averages of grid points over the same four sites and are plotted with a time lag of 1.5 h. For clarity only the TKE-PLACE model run is identified. The other seven model runs are plotted as small "+" symbols.

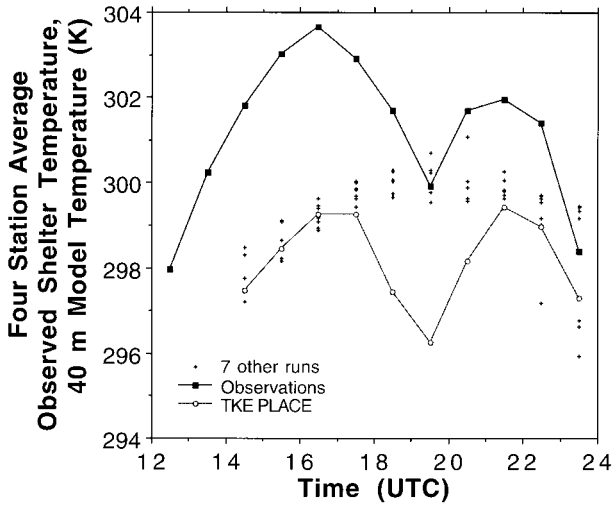

FIG. 11. Same as Fig. 10, but for surface temperature.

with small "+" symbols are the results of the seven other runs (not identified individually for clarity). The model results are lagged 1.5 h in the figure. This would not be expected to produce agreement between model and observations if the physical mechanisms generating the storm were different from the real mechanisms. However, one finds reasonably good agreement in Fig. 10. All model results seem to reproduce the transition from land breeze to sea breeze at these four stations. The slight high wind bias of the model results may be attributable to the difference between observation height and the height of the lowest model level. There is no obvious signature of the 1800 UTC storm in the wind field, as the sea breeze appears to continue to strengthen until late afternoon when the squall line arrives. Note that a minority of the other model runs also simulate the late afternoon return to westerly winds. But a majority of them sustain a sea breeze to the end of the simulation.

Plotted in Fig. 11 are the surface temperature observations and the model temperature at ~40 m AGL. Note that all model simulations display a significant cold temperature bias, for reasons discussed earlier. Under all but the lightest wind conditions with strong superadiabatic lapse rates, only about 0.4 K of this is caused by the difference in height above ground represented by the two curves. Most prominent in this figure is the very significant dip in surface temperature after midday, which is very well duplicated by the TKE-PLACE run but is entirely absent in the other seven runs. This dip is very likely caused by downdrafts from the observed storm. Other causes can contribute to this marked cooling, for example, the shading produced by the cloud, and perhaps even an enhanced influx of maritime air caused by the storm's convergence during its developing stage. Because all three model modifications were required to generate this storm within MM5, isolating the specific reasons for the model's accurate prediction might be best done by a process of elimination. The effect of the soil moisture anomaly would produce the storm in only four runs. Two more of those are eliminated if one assumes that SLAB is not able to generate realistic surface meteorology (see Table 3, wherein the ensemble of SLAB runs produces the poorest performance over the PAM network stations). Finally, in hourly analyses of the surface data from each of the model runs (not shown) it appears that the HIR-PLACE run came very close to generating this storm. A precursor area of local convergence is found in the precise location where the storm formed (not even this convergence zone is apparent in the other six runs). The fact that the storm did not form in this run may be attributable to the factor already discussed, that HIR cannot adequately handle the vertical moisture transport through the top of its diagnosed boundary layer, which is generally around cloud base, and into the cloud.

b. Sensitivity tests

Tables 2–4 show that TKE-PLACE produced the highest combined ranking of all simulations. TKE-PLACE did better than TKE-SLAB, which had the PLACE boundary conditions. This suggests the importance of including a vegetation model in these simulations. Also, TKE-PLACE 0 did better then TKE-SLAB 0, further showing the superiority of PLACE. The modeled improvement was very similar, in the net, for changes to the code or to the initialization. Below, we discuss in more detail differences among these groupings of runs. Factor separation analysis is used to

explain model sensitivities, where the factors are simply the changes to the model: (i) the PLACE offline derived soil moisture and temperature fields, (ii) the PLACE land surface model, and (iii) the TKE boundary layer scheme.

1) Importance of PLACE

Table 2 shows that the four simulations with PLACE ranked higher than simulations with SLAB. The simulations with PLACE had the lowest biases. These ensemble results confirm that PLACE is the most important change required to improve the simulation of surface meteorology over the entire peninsula, because it produced the highest aggregate ranking of any of the other ensembles. In regard to rainfall (Table 3) the change to TKE is by far the most important, as discussed earlier. But PLACE clearly outperformed SLAB. Similarly, in Table 4, the simulations with PLACE outperform SLAB. However, in simulating cloud amount both the change to TKE and the change to the case-specific initialization produce a more significant improvement.

2) Importance of initial soil boundary conditions

Tables 2–4 all show that simulations with the PLACE-derived, case-specific initialization did better than simulations with climatology (cf. the ''1'' and ''0'' rows). These results provide a generalized confirmation of previous findings that surface conditions feed through the boundary layer to have a noticeable impact on processes that form clouds and rain. Of course one must be cautious about extending these results beyond this specific case. Further case studies are required, particularly to study very different environments, in order to generalize these results. In winter cases, for example, dynamic processes might be expected to overwhelm any role played by surface initialization.

3) Importance of TKE

Experiments with TKE produced better mean wind direction over all PAM sites than any of the other groups of simulations (Table 2), but overall, the ensemble of four HIR runs did a better job of simulating surface meteorology than TKE for the 12-h daytime period at these 37 stations concentrated near Cape Canaveral. Although these results may not be representative of the entire domain, it is the only contrary result found in Tables 2–4, that is, the only result in which the incorporation of one of the model changes produced inferior results in some variables. Given that the same TKE ensemble does so much better at simulating clouds and rain (Tables 3 and 4), and that there is an overall model cold temperature bias that worsens as more cloud develops in the model, this result is probably at least partially rooted in some aspect of the cloud shortwave radiation scheme, as discussed earlier. Since HIR runs develop much less cloud and precipitation, they are less affected by a cold bias generated by model clouds that are too opaque/reflective. Also, the methodology used to create Table 2 can interpret errors in model timing of convection as large bias errors when the observations and model results are out of phase. Examination of Figs. 10 and 11 shows that when timing errors are accounted for, TKE-PLACE is far superior to the other runs in simulating the surface meteorology trends.

4) Factor separation analysis

To better elucidate the importance of the three separate model changes explored in this paper [1) Offline PLACE initialization vs climatology, 2) PLACE vs SLAB, 3) TKE vs HIR], we used the factor separation technique of Stein and Alpert (1993). The factor separation technique can be used to quantify individual and joint (or synergistic) contributions from changes to model processes (i.e., factors) that affect simulations (e.g., Alpert and Tsidulko 1994). Factor separation for three factors requires eight (2^3) simulations (Table 1). Of course, model simulation results depend on many other factors beside those chosen here. The MM5 run with only these ''unnamed'' factors is defined as the ''zero'' contribution. This is hereafter referred to as the control case, simulation HIR-SLAB 0.

The eight contributions are calculated as follows (X is any contribution and Y is a simulation):

$$X(0) = Y_{\text{HIR-SLAB 0}} \tag{1}$$

$$X(1) = Y_{\text{HIR-SLAB}} - Y_{\text{HIR-SLAB 0}} \tag{2}$$

$$X(2) = Y_{\text{HIR-PLACE 0}} - Y_{\text{HIR-SLAB 0}} \tag{3}$$

$$X(3) = Y_{\text{TKE-SLAB 0}} - Y_{\text{HIR-SLAB 0}} \tag{4}$$

$$X(1, 2) = Y_{\text{HIR-PLACE}} + Y_{\text{HIR-SLAB 0}} - (Y_{\text{HIR-SLAB}} + Y_{\text{HIR-PLACE 0}}) \tag{5}$$

$$X(1, 3) = Y_{\text{TKE-SLAB}} + Y_{\text{HIR-SLAB 0}} - (Y_{\text{HIR-SLAB}} + Y_{\text{TKE-SLAB 0}}) \tag{6}$$

$$X(2, 3) = Y_{\text{TKE-PLACE 0}} + Y_{\text{HIR-SLAB 0}} - (Y_{\text{HIR-PLACE 0}} + Y_{\text{TKE-SLAB 0}}) \tag{7}$$

$$X(1, 2, 3) = Y_{\text{TKE-PLACE}} - Y_{\text{HIR-SLAB 0}} - (Y_{\text{TKE-SLAB}} + Y_{\text{HIR-PLACE}} + Y_{\text{TKE-PLACE 0}}) + (Y_{\text{HIR-SLAB}} + Y_{\text{HIR-PLACE 0}} + Y_{\text{TKE-SLAB 0}}). \tag{8}$$

Note that any one of the seven other runs could arbitrarily be defined as the control run instead of HIR-SLAB 0.

Convective development is enhanced by air temperature contrast, whether between land and ocean or across different land surfaces. We define these temperature per-

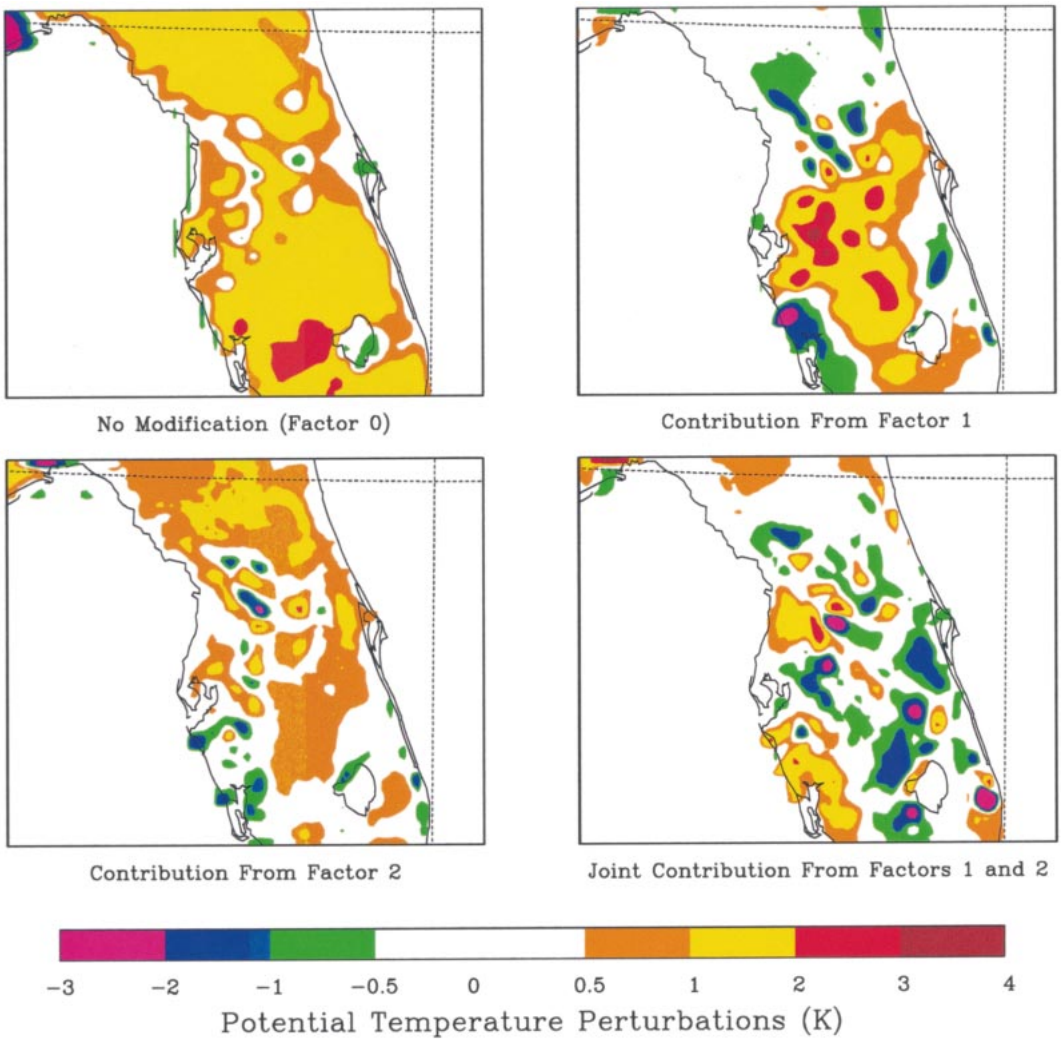

FIG. 12. Three contributions to the distribution of surface temperature perturbations ($X_{\theta'}$) and one joint contribution, at 1700 UTC. Only perturbations over land are shown although the perturbations are defined relative to an average potential temperature for the lowest model layer over the whole fine-mesh domain. The top left panel shows the contributions to θ' from the control version of MM5 (HIR-SLAB 0). The contributions from the PLACE offline initialization (Fig. 1) are in the top right panel. The contribution from the PLACE model appears at lower left, and the joint contribution from PLACE and its initialization are at lower right.

turbations, θ', by subtracting the lowest model level (~40 m) potential temperature at a point from the domain-averaged potential temperature. We examine the 1700 UTC data since this was after the development of the unstable boundary layer but prior to significant development of deep clouds in the model simulations. The contributions to the perturbation fields are referred to as $X_{\theta'}$ (i) where i indicates the factors [Eqs. (1)–(8)] used to calculate θ'.

The PLACE model and the PLACE offline soil initialization are the two primary factors that contribute to θ'. Therefore we present only these two factors, yielding four contributions to θ', which are shown in Fig. 12. In the control case, $X_{\theta'}(0)$ has, with one exception, maxima of 1–2 K over most of the peninsula. The relatively uniform initial soil moisture field (Fig. 1a) produced a nearly uniform field of perturbations. In contrast, the contribution from the PLACE offline initial conditions, $X_{\theta'}$ (1), correlated closely with the spatial distribution of dry soil (Fig. 1b) and produced maxima as large as 4 K. The most important effect of the joint interaction of both factors occurred over west-central Florida. This region showed relatively large values of $X_{\theta'}$ (1, 2) ranging up to 3 K. The combination of relatively small soil moisture and vegetation led to warming of the surface layer to a degree not produced by either factor alone.

The development of cloud condensate depends upon the vertical transport of heat and moisture. One measure of this is the dewpoint (DP). We examine the dewpoint at ~1.5 km above the surface at 1700 UTC. Figure 13 shows that contributions from the control, the initial soil moisture, and PLACE [i.e., X_{DP} (0), X_{DP} (1), and X_{DP}

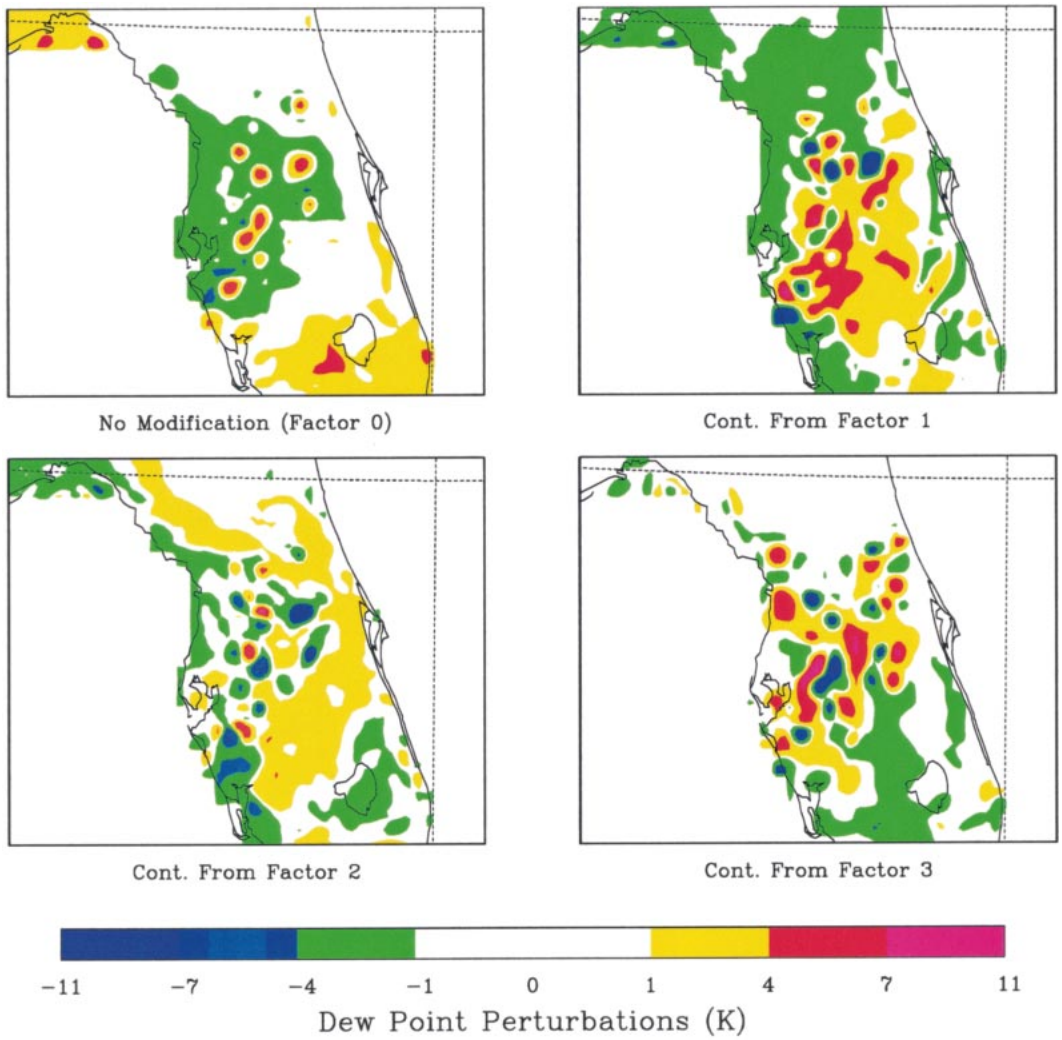

FIG. 13. Single contributions to dew point temperature distribution at 1.5 km above the surface at 1700 UTC. The perturbations were defined relative to an average dewpoint over the peninsula.

(2)] have a spatial pattern very similar to the surface heating in each case. Notably, X_{DP} (3) (TKE) had maxima along the southwest coast and in the center of the peninsula. This confirms the earlier discussion of Tables 3 versus 4, where HIR performs better than TKE in modeling the surface meteorology over the eastern side of the peninsula. In the area of the PAM mesonetwork, TKE-SLAB 0 shows no perturbation relative to HIR-SLAB 0, whereas in other parts of the domain, TKE-SLAB 0 produced large positive dewpoint perturbations at 1.5 km. This suggests, as discussed earlier, that the TKE parameterization is able to link the boundary layer/subcloud layer with the nascent convective clouds that were forming at 1700 UTC (Fig. 2), whereas HIR artificially inhibits this link.

To further explore the importance of the three separate model changes, we now examine their contributions to vertically averaged cloud condensate. Each contribution is referred to as $X_{\psi'}(i)$. Figure 14 shows that modifying the model physics by changing the surface initialization [$X_{\psi'}$ (1)] or by changing the land parameterization [$X_{\psi'}$ (2)] produced relatively little effect on the modeled cloud condensate at 1800 UTC. However, $X_{\psi'}$ (1, 2) shows that these two factors can weakly combine to enhance cloud condensate near Lake Okeechobee and along the southeast coast.

The factor $X_{\psi'}$ (3) shows that TKE (alone) contributes a small increase in cloud condensate. The importance of TKE can be more readily seen when TKE acts jointly with other factors. For example, comparing $X_{\psi'}$ (1, 2) with $X_{\psi'}$ (1, 3) shows that the addition of a more realistic boundary layer is more important than the addition of a more realistic land scheme. Comparing $X_{\psi'}$ (1, 3) and $X_{\psi'}$ (2, 3) shows that adding the TKE factor with the PLACE offline initialization produces more cloud than applying TKE with the PLACE model alone. However,

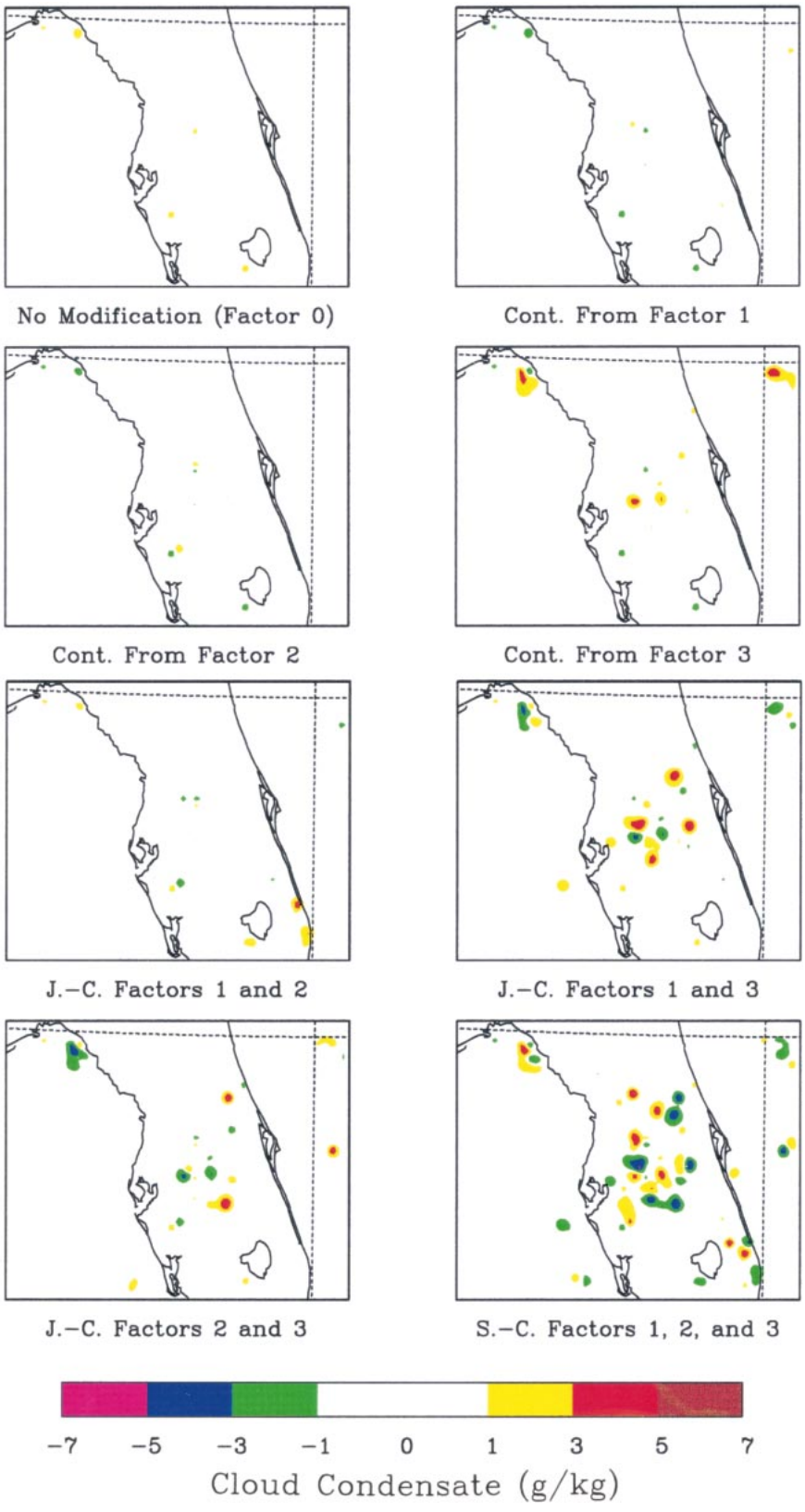

FIG. 14. Single, joint (''J.-C.'') and synergistic (''S.-C.'') contributions to cloud condensate (referred to as $X_{\psi'}$ in the text) at 1800 UTC.

$X_{\psi'}$ (1, 2, 3) shows that all three factors combine synergistically to produce the largest impact on cloud condensate.

Thus the differences between Figs. 7 and 8, when explored in more detail using the factor separation technique, can be seen to involve synergistic interactions (presumably nonlinear) between all three of the model changes examined in this paper. This is an important result that is likely to be applicable to any coupling of a physical parameterization to an atmospheric model. There are important interactions between physical parameterizations that can significantly affect the performance of the newly coupled parameterization. It is suggested that adequate evaluation of the new parameterization requires evaluation of its interactions with multiple choices of other parameterizations, as is performed here.

5. Summary and conclusions

This study demonstrated improvements to the MM5 model by coupling with it an improved 1.5-order closure turbulence parameterization scheme (TKE), a state-of-the-art soil–vegetation land model (PLACE), and the soil moisture and temperature initialization provided by running PLACE offline a priori. We compared an ensemble of eight model simulations, incorporating all combinations of the three changes, both qualitatively and quantitatively to observed data. Overall, the TKE-PLACE model produced more realistic results than the control model (HIR-SLAB 0), including a better simulation of the sensible heat flux, lower biases for an aggregate of surface meteorology variables, better rainfall, and more realistic cloud fraction.

Sensitivity tests showed that the physical representation of the boundary layer and land surface affects the model results quite strongly. A factor separation analysis first demonstrated the importance of two factors: the initial soil temperature and moisture, and the PLACE land model. The initial soil temperature and moisture fields determine the general spatial structure of the surface temperature perturbations, while PLACE (e.g., its explicit treatment of vegetation) can strongly modify these fields. Note that PLACE allows soil moisture to evolve in time during a model simulation. Simpler models such as SLAB do not allow this, nor do they explicitly contain a vegetation layer. Additional analysis showed the importance of the third factor, TKE. The MM5 model required the combined, synergistic effect of all three factors to produce its most realistic simulation.

The addition of the new model subcomponents could likely have additional benefits to mesoscale weather and local climate prediction. Sophisticated land models such as PLACE and higher-order closure models such as TKE should have their greatest benefit in predicting warm season, weakly forced convection, including land–sea breezes, mountain–valley breezes, and airmass thunderstorms. Land processes may also play a role in modifying storms more strongly forced by large scale dynamic processes as well. PLACE can provide more realistic surface boundary conditions, including the time evolution of soil moisture and temperature (as well as runoff) than simple SLAB models. TKE can provide better transport of moisture, heat, and momentum through the PBL and within clouds than first-order closure schemes. This is especially important at fine scales where convection cannot be parameterized.

This study evaluated a single case and compared only two land models, two boundary layer/turbulence parameterizations, and two soil moisture/temperature initializations. Further testing is imperative to gain added confidence in the model performance. Tests involving varying the vegetation cover, initial conditions over the ocean, the MRF boundary layer scheme, and other land surface parameterizations should be given high priority in future work.

Finally, the simulations produced here used a relatively fine 5-km resolution without the added complication of a very important and strongly interacting fourth factor: the cumulus parameterization scheme. Additional studies are under way to test the importance of all four factors at resolutions more suited to future regional climate studies and continental-scale mesoscale model simulation, that is, 25–100 km.

Acknowledgments. The first author was supported by a National Aeronautics and Space Administration Cooperative Agreement NCC 5-82. He thanks Robert Adler and Bill Lau for their support. He would also like to thank Harry Cooper for supplying the flux and PAM data from the CaPE experiment site, and Jeff Halverson for providing advice on the CaPE experiment. W.-K. Tao, R. D. Baker, and Y. Jia are supported by NASA headquarters' (HQ) physical climate program and TRMM. They thank R. Kakar (HQ) for his support. We would also like to thank an anonymous reviewer for comments that led to significant improvements in the paper. The views expressed herein are those of the authors and do not necessarily reflect the views of Columbia University, The Pennsylvania State University, NASA, or Tel Aviv University.

REFERENCES

Alpert, P., and M. Tsidulko, 1994: Project Wind—numerical simulation with Tel Aviv Model PSU-NCAR model run at Tel Aviv University. *Mesoscale Modeling of the Atmosphere, Meteor. Monogr.,* No. 47, Amer. Meteor. Soc., 81–95.

Atkins, N. T., R. M. Wakimoto, and T. M. Weckwerth, 1995: Observations of the sea-breeze front during CaPE. Part II: Dual-Doppler and aircraft analysis. *Mon. Wea. Rev.,* **123,** 944–969.

Avissar, R., and F. Chen, 1993: Development and analysis of prognostic equations for mesoscale kinetic energy and mesoscale (subgrid-scale) fluxes for large scale atmospheric models. *J. Atmos. Sci.,* **50,** 3751–3774.

Barnes, S. L., 1964: A technique for maximizing details in numerical weather map analysis. *J. Appl. Meteor.,* **3,** 396–409.

Blanchard, D. O., and R. E. Lopez, 1985: Spatial patterns of convection in south Florida. *Mon. Wea. Rev.*, **113,** 1282–1299.

Boone, A., and P. J. Wetzel, 1996: Issues related to low resolution modeling of soil moisture: Experience with the PLACE model. *Global Planet. Change,* **13,** 161–181.

——, and ——, 1999: A simple scheme for modeling sub-grid soil texture variability for use in an atmospheric climate model. *J. Meteor. Soc. Japan,* **77,** 317–333.

Boybeyi, Z., and S. Raman, 1992: A three-dimensional numerical sensitivity study of convection over the Florida peninsula. *Bound.-Layer Meteor.,* **60,** 325–359

Byers, H. R., and H. R. Rodebush, 1948: Causes of thunderstorms of the Florida peninsula. *J. Meteor.*, **5,** 275–280.

Chang, J.-T., and P. J. Wetzel, 1991: Effects of spatial variations of soil moisture and vegetation on the evolution of a pre-storm environment: A numerical case study. *Mon. Wea. Rev.,* **119,** 1368–1390.

Chen, Y.-L., and J.-J. Wang, 1995: the effects of precipitation on the surface temperature and airflow over the island of Hawaii. *Mon. Wea. Rev.,* **123,** 681–694.

Dudhia, J., 1993: A nonhydrostatic version of the Penn State–NCAR mesoscale model: Validation tests and simulation of an Atlantic cyclone and cold front. *Mon. Wea. Rev.,* **121,** 1493–1513.

Fankhauser, J. C., N. A. Crook, J. Tuttle, L. J. Miller, and C. G. Wade, 1995: Initiation of deep convection along boundary layer convergence lines in a semi-tropical environment. *Mon. Wea. Rev.*, **123,** 291–313.

Gayno, G. A., 1994: Development of a higher-order, fog producing boundary layer model suitable for use in numerical weather prediction. M. S. thesis, Dept. of Meteorology, The Pennsylvania State University, 104 pp. [Available from the Dept. of Meteorology, The Pennsylvania State University, University Park, PA 16802.]

Grell, G. A., J. Dudhia, and D. R. Stauffer, 1994: A description of the fifth-generation Penn State/NCAR Mesoscale Model (MM5). NCAR Tech. Note NCAR/TN-398+STR, 122 pp.

Halverson, J., M. Garstang, J. Scala, and W.-K. Tao, 1996: Water and energy budgets of a Florida mesoscale convective system: A combined observational and modeling study. *Mon. Wea. Rev.*, **124,** 1161–1180.

Hong, S.-Y., and H.-L. Pan, 1996: Nonlocal boundary layer diffusion in a medium-range forecast model. *Mon. Wea. Rev.*, **124,** 2322–2339.

Kain, J. S., and J. M. Fritsch, 1990: A one-dimensional entraining/detraining plume model and its application to convective parameterization. *J. Atmos. Sci.,* **47,** 2784–2802.

Kingsmill, D. E., 1995: Convection initiation associated with a seabreeze front, a gust front, and their collision. *Mon. Wea. Rev.*, **123,** 2913–2933.

Lynn, B. H., W.-K. Tao, and P. J. Wetzel, 1998: A study of landscape-generated deep moist convection. *Mon. Wea. Rev.,* **126,** 928–942.

Lyons, W. A., C. J. Tremback, and R. A. Pielke, 1995: Applications of the Regional Atmospheric Modeling System (RAMS) to provide input to photochemical grid models for the Lake Michigan Ozone Study (LMOS). *J. Appl. Meteor.,* **34,** 1762–1786.

Mahrt, L., J. S. Sun, D. Vickers, J. I. MacPherson, J. R. Pederson, and R. L. Desjardins, 1994: Observations of fluxes and inland breezes over a heterogeneous surface. *J. Atmos. Sci.,* **51,** 2484–2499.

Meeson, B. W., and Coauthors, 1995: ISLSCP initiative I—Global data sets for land–atmospheric models, 1987–1988. Volumes 1–5, Published on CD by NASA (USA_NASA_GDAAC _ISLSCP_001–USA_NASA_GDAAC_ISLSCP_005).

Nicholls, M. E., R. A. Pielke, and W. R. Cotton, 1991: A two-dimensional numerical investigation of the interaction between sea breezes and deep convection over the Florida peninsula. *Mon. Wea. Rev.,* **119,** 298–323.

Pielke, R. A., 1974: A three-dimensional numerical model of the sea breezes over south Florida. *Mon. Wea. Rev.*, **102,** 115–119.

——, 1984: *Mesoscale Numerical Modeling.* Academic Press, 612 pp.

——, G. A. Dalu, J. S. Snook, T. J. Lee, and T. G. F. Kittel, 1991: Nonlinear influence of mesoscale land use on weather and climate. *J. Climate,* **4,** 1053–1069.

——, T. J. Lee, J. H. Copeland, J. L. Eastman, C. L. Ziegler, and C. A. Finley, 1997: Use of USGS-provided data to improve weather and climate simulations. *Ecol. Appl.,* **7,** 3–21.

——, R. L. Walko, L. T. Steyaert, P. L. Vidale, G. E. Liston, W. A. Lyons, and T. N. Chase, 1999: The influence of anthropogenic landscape changes on weather in south Florida. *Mon. Wea. Rev.,* **127,** 1653–1673.

Shafran, P. C., N. L. Seaman, and G. A. Gayno, 2000: Evaluation of numerical predictions of boundary layer structure during the Lake Michigan Ozone Study. *J. Appl. Meteor.,* **39,** 412–426.

Shaw, B. L., R. A. Pielke, and C. L. Ziegler, 1997: A three-dimensional numerical simulation of a Great Plains dryline. *Mon. Wea. Rev.,* **125,** 1489–1506.

Stauffer, D. R., and N. L. Seaman, 1999: Intercomparison of turbulence parameterizations for simulating coastal-zone marine boundary layer structure. Preprints, *Third Conf. on Coastal Atmospheric and Oceanic Prediction Processes,* New Orleans, LA, Amer. Meteor. Soc., 2–7.

——, R. C. Muñoz, and N. L. Seaman, 1999: In-cloud turbulence and explicit microphysics in the MM5. Preprints, *Ninth MM5 Users Workshop,* Boulder, CO, National Center for Atmospheric Research, 177–180.

Stein, U., and P. Alpert, 1993: Factor separation in numerical simulations. *J. Atmos. Sci.,* **50,** 2107–2115.

Watson, A. I., and D. O. Blanchard, 1984: The relationship between total area divergence and convective precipitation in south Florida. *Mon. Wea. Rev.,* **112,** 673–685.

Wetzel, P. J., and A. Boone, 1995: A parameterization for land–atmosphere–cloud exchange (PLACE): Documentation and testing of a detailed process model of the partly cloudy boundary layer over heterogeneous land. *J. Climate,* **8,** 1810–1837.

Wilson, J. W., and D. L. Megenhardt, 1997: Thunderstorm initiation, organization, and lifetime associated with Florida boundary layer convergence lines. *Mon. Wea. Rev.,* **125,** 1507–1525.

Xu, L., S. Raman, R. V. Madala, and R. Hodur, 1996: A non-hydrostatic modeling study of surface moisture effects on mesoscale convection induced by sea breeze circulation. *Meteor. Atmos. Phys.,* **58,** 103–122.

Zhang, D. L., and R. A. Anthes, 1982: A high resolution model of the planetary boundary layer: Sensitivity tests and comparisons with SESAME-79 data. *J. Appl. Meteor.,* **21,** 1594–1609.